Journal of the European Ceramic Society **18** (1998) 837–848

PII: S0955-2219(97)00000-0
0955-2219/98/$19.00 + 0.00

Processing–Microstructure–Property Relations in Mullite–Cordierite Composites

T. Ebadzadeh and W. E. Lee

Department of Engineering Materials, University of Sheffield, Sheffield, UK

(Received 28 July 1997; accepted 7 November 1997)

Abstract

The complex interrelations between processing, microstructure and electrical and mechanical properties are considered for mullite–cordierite composites. Fabrication procedures using mixed powders or routes based on sol–gel precursors are presented, along with the phase evolution, densification and microstructural formation. Final microstructures (including porosities and grain sizes) are correlated to the mechanical (hardness, toughness and strength) and electrical (dielectric constant) properties.

1 Introduction

Mullite–cordierite composites not only have good high-temperature properties but also excellent electrical insulating ability making them potentially useful in applications ranging from refractories to computer substrates. A variety of routes have been used for their manufacture such as using mixed, pre-made mullite and cordierite powders,[1–3] mullite powder and cordierite composition glass,[2,4] combustion synthesis[5] and mixed mullite and cordierite sols.[6] The complex crystal structures and chemical constitution of such aluminosilicates makes mass transport and so solid state sintering slow. Consequently, in multiphase aluminosilicate bodies made from premade phases densification does not occur readily until a eutectic temperature, or the melting temperature of one of the components, is reached. Many of these elaborate processing routes seek to overcome this difficulty by inducing densification before formation of the desired phases.

A complicating factor in this system is the range of stoichiometry of the mullite and cordierite phases. Mullite (orthorhombic, space group Pbam) has a defect structure based on oxygen vacancies which accommodates the nonstoichiometry and the average composition may range from close to $3Al_2O_3.2SiO_2$ to $3Al_2O_3.SiO_2$. These oxygen vacancies can order to varying degrees and high alumina mullites are often referred to as having a tetragonal structure because e.g. of the absence of 120/210 peak splitting. However, it is now believed[7] that these mullites are orthorhombic and the diffraction information is a direct result of ordered domains and twinning so that such mullite should strictly be referred to as pseudo-tetragonal. Mullite can also be prepared by sol–gel routes with up to 1·5wt% MgO in solid solution.[8] The polymorphism and stoichiometry of cordierite ($2MgO.2Al_2O_3.5SiO_2$) is also complicated. For *stoichiometric* cordierite the high-temperature form, high cordierite or indialite (α) is hexagonal (space group P6/mcc) and can be made by solid state reaction of mixed oxides between 1300–1460°C although it is metastable below 1450°C slowly transforming to β or low cordierite (orthorhombic, space group Cccm). The other polymorph is μ also confusingly termed β-quartz or high quartz solid solution because Al^{3+} substitutes for Si^{4+} in the high quartz crystal structure with Mg^{2+} 'stuffed' into the structure to allow charge compensation. μ-cordierite is hexagonal with space group $P6_222$ and metastable but common on crystallising cordierite composition glass below 1000°C.[9] *Off-stoichiometric* compositions of cordierite itself can occur with stoichiometry ranging from $2MgO.2Al_2O_3.5SiO_2$ towards compositions richer in MgO and SiO_2 [10] although high MgO/SiO_2 contents stabilise the orthorhombic β form.[11] μ-cordierite phases occur with a considerable range of solid solution.[12] These β-quartz solid solutions (or μ-cordierites) have compositions $MgO.Al_2O_3.xSiO_2$ (where $x = 2–10$) and commonly form on crystallising glass, later transforming to α only after sufficient diffusion has occurred for $2MgO.2Al_2O_3.5SiO_2$ composition to be achieved.

In the present study, mullite–cordierite composites were prepared by two methods: (1) from a mixture of precursors, and (2) from a mixture of premade mullite and cordierite powders. The

precursor powders were calcined at low temperatures (600 and 950°C) to facilitate densification due to the presence of highly reactive phases such as γ-alumina and amorphous silica and sintering via viscous flow. Crystallisation, densification behaviour, and microstructural development of mullite–cordierite composites prepared from these different starting materials were examined. Mechanical and dielectric properties were measured and related to the observed microstructures.

2 Experimental Procedure

2.1 Preparation of mullite and cordierite powders and composites from mixed powders

The starting materials used to produce mullite–cordierite composites derived from powders were mullite and cordierite powders prepared from reagent grade $Al_2(SO_4)_3.16H_2O$, and colloidal silica and $Mg(NO_3)_2.6H_2O$.[13] Figure 1 shows the processing route for mullite and cordierite powders, and mixed mullite and cordierite powders (composites). Pure cordierite powder was calcined 2 h at 1300°C while pure mullite powder was calcined for 2 h at 1700°C. Mullite–cordierite composites with different proportions of mullite (10, 50 and 90 wt%, denoted as 19, 55 and 91, respectively) were prepared by mixing and milling calcined mullite and cordierite powders (denoted Ps) in a ball-mill, using zirconia media in ethanol, for 6 h. The resulting slurries were filtered and the cakes were dried at 90°C for 24 h, before grinding in an agate mortar with a pestle. The resulting powders were uniaxially pressed to 10 mm dia. $\times \approx 10$ mm height pellets at 250 MPa and sintered 2 h at temperatures ranging from 1300 to 1450°C.

2.2 Preparation of mixed mullite–cordierite precursors

Figure 2 shows the processing of mullite–cordierite composites derived from two types of precursor. In the first route (Sb) a mullite–cordierite composite precursor was made from reagent grade colloidal silica, boehmite and magnesium nitrate. The colloidal silica was diluted and magnesium nitrate dissolved separately in deionised water, while boehmite was dispersed in deionised water (added

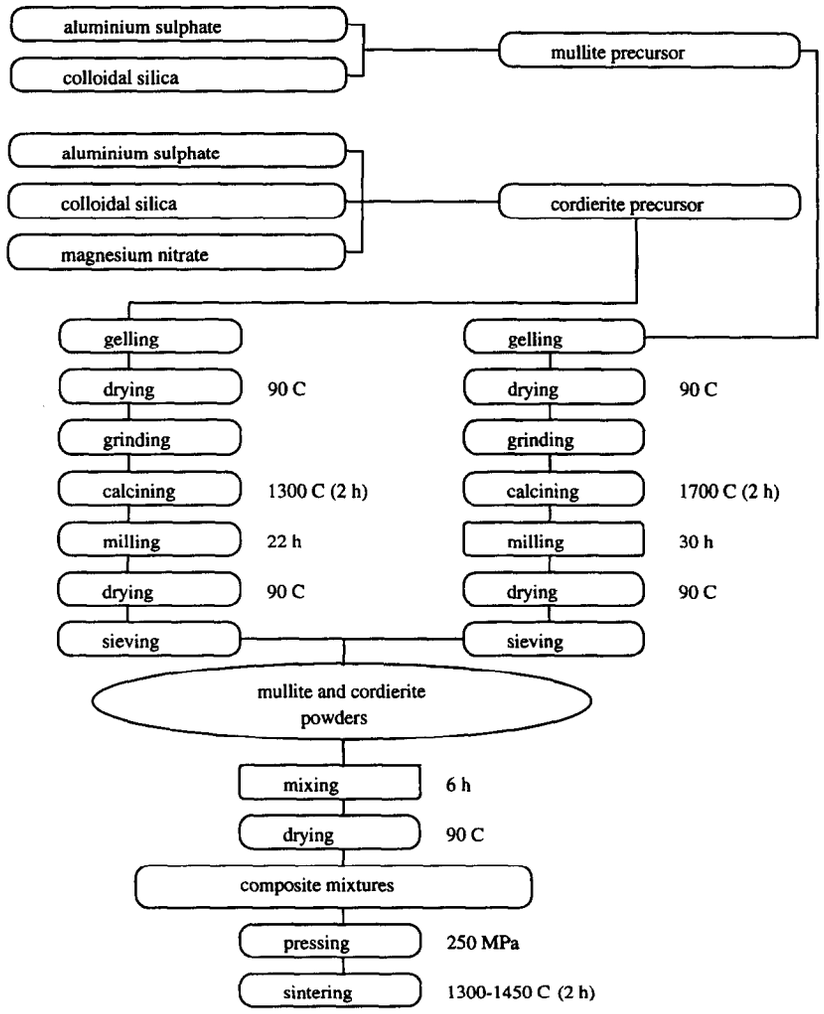

Fig. 1. Processing of mullite and cordierite powders and composite mixed powders.

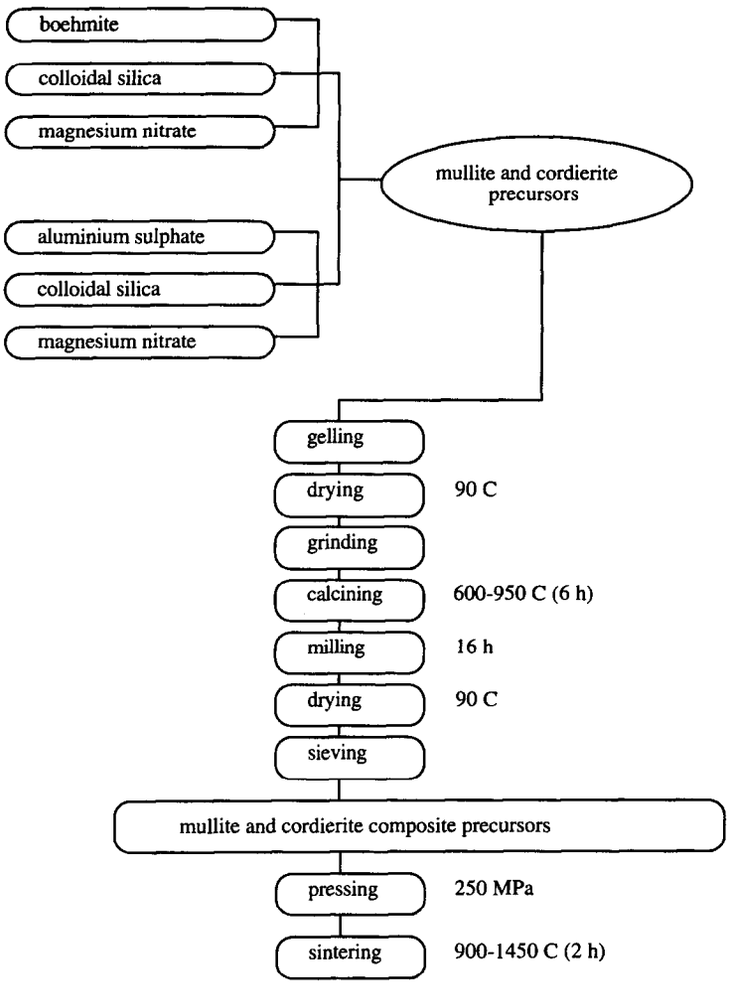

Fig. 2. Processing of mullite–cordierite composite mixed precursors.

vigorously to stirred water) by adjusting the pH to 3 with nitric acid. The concentration of particles in solution was adjusted by controlling the weight ratio of aluminium and magnesium sources and the silica/water ratio. The silica–sol followed by the magnesium solution were added to the dispersed boehmite while stirring vigorously. In the second route (Ss) a mullite–cordierite composite precursor was derived from reagent grade aluminium sulphate, colloidal silica and magnesium nitrate. It was prepared by dissolving aluminium sulphate and magnesium nitrate in deionised water, separately, and then adding the silica–sol prepared via the route described above and the dissolved magnesium nitrate to the aluminium solution while stirring vigorously. It is worth noting that the scale of mixing in aluminium-sulphate derived composites is in the nm range while for the boehmite derived composites this range increases to μm.

The solutions were evaporated at 90°C and the resulting gels were dried at 120°C for 6 h. Dried gels were ground, and calcined for 6 h at 600°C for boehmite containing dried gels (denoted Sb), and 6 h at 950°C for aluminium sulphate-containing dried gels (denoted Ss). X-ray diffraction (XRD) of these powders after calcination revealed small amounts of crystallisation had occurred (see Section 3.1). Calcined powders were milled for 16 h in a ball-mill, using zirconia media in ethanol and the resulting slurries were dried at 90°C. Dried precursor particles were screened through a 38 μm sieve, uniaxially pressed into 10 mm dia. $\times \approx 10$ mm height pellets at 250 MPa and sintered 2 h at temperatures ranging from 900–1450°C.

2.3 Characterisation techniques

Crystalline phase identification was performed on powders, made from ground sintered pellets, using X-ray diffraction (Philips powder diffractometer 1710) with Ni-filtered Cu-Kα radiation and the relevant JCPDS cards for orthorhombic 3:2 mullite (15-776), hexagonal α-cordierite (13-293), orthorhombic β-cordierite (13-294), hexagonal μ-cordierite (14-249), cubic γ-alumina (10-425), tetragonal cristobalite (11-695), and cubic spinel ($MgAl_2O_4$) (21-1152). Due to the difficulty of distinguishing the transition aluminas in complex phase mixtures they (i.e. δ, θ, etc) are all grouped together as γ-Al_2O_3. The presence of pseudotetragonal mullite was confirmed by the merging of

the 120/210 peaks of orthorhombic mullite.[7,14] Crystallisation of mullite and cordierite phases in each sintered composite was analysed by comparing the integrated intensity of (100), (202) and (211) peaks of α-cordierite, and (110), (001) and (220) peaks of orthorhombic mullite, peaks which are free of overlap. Scanning electron microscopy (SEM) was performed using a Camscan Series 2A instrument and the different phases distinguished using energy-dispersive spectroscopy (EDS) (Link AN 10000) and backscattered electron images. Transmission electron microscopy (TEM) was performed using Philips 400, 420 and Jeol 200 CX electron microscopes operating at 100, 120 and 200 kV, respectively. Densification behaviour of the green and sintered bodies was determined by the Archimedes technique. Porosity measurements of sintered samples were carried out according to ASTM-C373 (1969). Grain sizes of sintered pellets were determined using the linear intercept method[15] on thermally or HF etched pellets and particle size distributions of calcined powders were determined using a Coulter LS 130 laser particle size analyser and Dispex N40 as deflocculant (the optimum amount, i.e. giving the smallest particle size, was obtained for every run of the different powders).

2.4 Property measurements

Bend strength tests on rectangular cross section bars were carried out on an Instron machine at room temperature by using four-point bending with a 20 mm span between the inner rods and 40 mm span between the outer rods. The cross-head speed was 0·4 mm per min. The bar samples were prepared by pressing the powders in a bar shaped steel die at 250 MPa. After densification the bars were ground and polished with diamond paste (from 6 to 0·25 μm). The final bar dimensions were 48 mm × 9 mm × 4 mm.

A standard Leitz miniload hardness tester was used to obtain the Vickers hardness values, using a load of 1 Kg. Toughness measurements were made using the indentation technique of Evans and Charles.[16]

Dielectric constant measurements were made on disc-shaped samples, (9–10 mm diameter and $\approx$ 1 mm thickness). All measurements were undertaken at room temperature and 1 MHz on a Hewlett Packard HP4284A Precision LCR meter, with a frequency range from 20 Hz–1 MHz. In estimating the dielectric constants of the composites, the dielectric constants of fully mullite (sintered 2 h at 1700°C) and cordierite (sintered 2 h at 1400°C) ceramics were measured. After normalising to zero porosity by dividing the measured values by a factor (1–P), where P is the pore fraction, values of 7·2 and 5·0 were obtained, for pure mullite and cordierite, respectively.

3 Results and Discussion.

3.1 Crystallisation

Results of XRD analysis of the composite powders and precursors are shown in Table 1. The early stages of crystallisation of the precursor samples (Sb and Ss) are of interest since they influence the reactivity of the resulting powder. Crystallisation from the amorphous precursors began during the calcination treatments, i.e. in the boehmite-based (Sb) samples (Sb 55) at 600°C and at 950°C in the aluminium sulphate-based systems (Ss). After 6 h at 600°C γ-Al_2O_3 peaks appear in Sb55 and after 2 h at 950°C Ss55 shows small peaks from pseudo-tetragonal mullite, β-cordierite, γ-Al_2O_3 and $MgAl_2O_4$ spinel. After 2 h at 1100°C (Table 1) the Ss samples still reveal pseudo-tetragonal mullite, β-cordierite and γ-Al_2O_3 along with $MgAl_2O_4$ spinel in the cordierite-rich samples (Ss19, Ss55). Spinel is often observed in sol–gel cordierites when the gel is heterogeneous along with β-cordierite.[17] On the other hand, in the boehmite-based (Sb) samples only γ-Al_2O_3 appears and also spinel in the 50% mullite sample (Sb55). By 1200°C in the Ss system the spinel has disappeared, orthorhombic mullite has formed and cristobalite crystallised (except in Ss91). In the Sb system at this temperature many of the phases formed at lower temperature in Ss appear such as β-cordierite, spinel (in cordierite-rich samples Sb19, Sb55) and mullite (although orthorhombic). Cristobalite also crystallises in all Sb samples at 1200°C consistent with Wei and Hallorans[18] observation of spinel in non-stoichiometric mullite prepared by the Sb route. It should be emphasised that while crystallisation of these phases is detected at the temperatures described above the samples are still predominantly amorphous. Sb samples below 1200°C and Ss below 1100°C are still mostly glass as are the calcined starting materials themselves. The observation of β-cordierite at 1200°C but α-cordierite at 1300°C and above also needs further discussion since at these temperatures in stoichiometric cordierite the β form would be thermodynamically stable. EDS analysis in the TEM[13] confirmed that the β-cordierite formed at 1200°C contained MgO consistent with the stabilisation of this phase by MgO observed by Smart and Glasser[11] while the α-cordierite formed at 1300°C contained no detectable MgO. The MgO present in the system has stabilised the β form in a cordierite solid solution at the lower temperature although not at 1300°C. By 1300°C both powder and precursor samples (Ps, Sb and Ss) are orthorhombic mullite, α-cordierite mixtures and further heating improves the crystallinity of these two phases.

In all the 90% mullite compositions, the α-cordierite peaks disappeared after 2 h at 1450°C. It seems likely that this is because the cordierite has melted incongruently to form mullite and liquid. While 1450°C is below the melting temperature of stoichiometric cordierite (1460°C), as pointed out by Smart and Glasser,[11] solution with MgO decreases its melting temperature. The low total MgO in these 90% mullite compositions means they are then so depleted in MgO, since up to 1·5% of it can go into solution in the mullite,[8] that cordierite crystallisation on cooling does not occur. In Ss91 it is believed that at an early stage most of the cordierite precursor forms mullite with MgO in solid solution because only small cordierite peaks could be detected by XRD. MgO is known to decrease the mullitisation temperature in sol–gel derived mullites[8] and this will be discussed further in Section 3.3.

3.2 Densification

Figures 3–5 show the composites densification behaviour. For the precursor route, densification of Sb composites occurs at lower temperature than for Ss composites at all sintering temperatures and mullite contents. The enhanced densification of composites derived from boehmite precursors is because most of the crystallisation occurs at higher temperature (at about 1200°C) and since crystallisation competes with densification for mass transport the higher crystallisation temperature gives more opportunity for viscous flow. Furthermore, in the Sb systems the glass formed may have a greater water content (derived from OH in the boehmite) which tends to increase its fluidity and improve densification. Once the phases crystallise, densification by this mechanism is limited. Another possible reason for enhanced densification of Sb composites was attributed to their higher packing density as suggested by green density measurements.[13] The green pellets derived from boehmite had higher bulk density (1·36 g cm^{-3}) than aluminium sulphate-derived green pellets (1·17 g cm^{-3}). The low packing density of Ss bodies could be attributed to the presence of large (> 10 μm) pore-containing aggregates formed in precursor powder after the 950°C calcination not observed in Sb precursor powders after the 600°C calcination. In all precursor-derived (Ss and Sb) composites, rapid densification arises after 2 h above 1000°C due to the high reactivity of the precalcined powders containing the amorphous silica and transient phases such as spinel and γ-alumina. Composites derived from powders (Figs 3–5) reached full density only after the cordierite melted. The wetting angle between mullite and molten cordierite ($\theta = 24°$)[2] limits penetration of mullite–mullite contacts unless substantial liquid is present

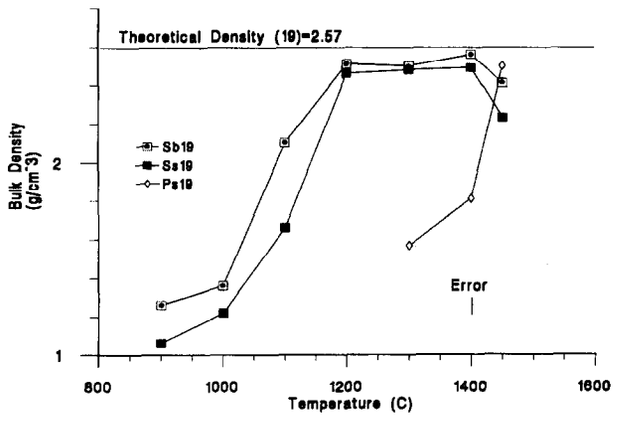

Fig. 3. Density of 10wt% mullite composites derived from powder Ps and precursors (Ss and Sb) held 2 h at temperatures indicated.

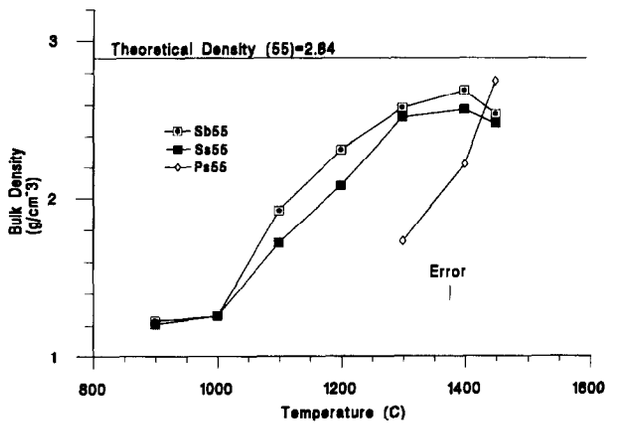

Fig. 4. Density of 50wt % mullite composites derived from powder Ps and precursors (Ss and Sb) held 2 h at temperatures indicated.

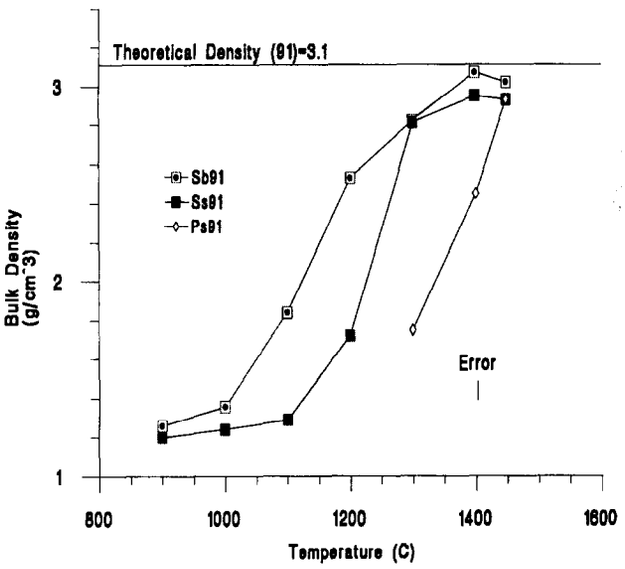

Fig. 5. Density of 90wt% mullite composites derived from powder Ps and precursors (Ss and Sb) held 2 h at temperatures indicated.

but even 10% cordierite samples appear to form sufficient liquid.

3.3 Microstructural evolution

Since maximum densities were obtained in the precursor route composites (Sb and Ss) after 2 h at 1400°C microstructures after sintering at these conditions will be emphasised although it is also of interest to briefly examine earlier stages in these composites to get some idea of how they evolve. On the other hand, reasonable densities are not achieved in the powder systems (Ps) until temperatures at which liquid forms so that microstructures from higher temperatures will be considered for these. Other microstructural features such as porosity and grain size are considered further in following sections. Figure 6 shows SEM images of *90% mullite composites* after 2 h at 1400°C. Ss composites clearly have a smaller grain size ($\approx 0{\cdot}5\,\mu$m average) than Sb ($\approx 1{\cdot}2\,\mu$m). Figure 7 shows bright field (BF) TEM images of these two compositions. The larger grain size in Sb is apparent [Fig. 7(b)] along with several other features including dislocations, dislocation networks and rounded cores which are mostly free of defects. EDS confirmed that the majority of these cores were mullite composition (although the exact stoichiometry was not determined). All grains containing cores also contained dislocations. This highly stressed microstructure contrasts with the stress-free Ss microstructure [Fig. 7(a)]. The different microstructures of these two composites are most likely related to the varying scales of mixing of the starting materials or trace levels of impurities such as sulphur in the sulphate-derived composite (Ss).

It seems likely that the dislocations formed during growth and densification associated with the formation of the mullite cores from reaction of the coarser starting materials, particularly boehmite, in Sb. The mullite cores may lead to dislocation formation due to different thermal expansion of the grain core and shell due to their different orientations, the thermal expansion coefficient of mullite being $4{\cdot}5\times10^{-6}\,K^{-1}$ along the **a** direction but $5{\cdot}7\times10^{-6}\,K^{-1}$ along the **c** direction from 25–1000°C. The thermal expansion mismatch between mullite and cordierite (whose thermal expansion coefficient is about $1\times10^{-6}\,K^{-1}$ 25–1000°C) may cause the formation of dislocations on cooling from the sintering temperature. However, this seems unlikely due to the small amount (10%) of

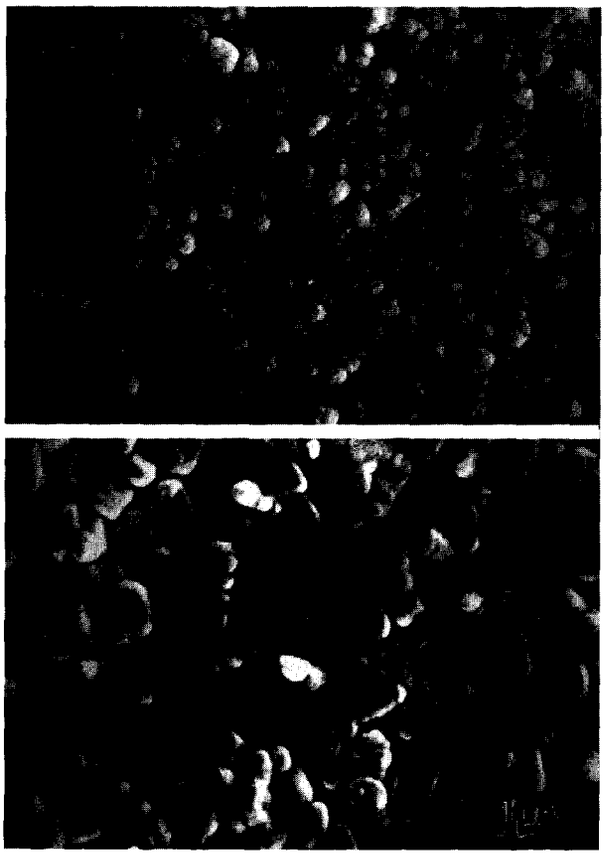

Fig. 6. SEM images of (a) Ss91 and (b) Sb91 composites sintered 2 h at 1400°C and thermally etched at 1300°C for 30 min.

Fig. 7. BF-TEM images of (a) Ss91 and (b) Sb91 sintered 2 h at 1400°C. The featureless mullite cores in most grains in Sb91 are arrowed, the angular features present in MgO-doped mullite grains in Ss91 are voids.

cordierite present and because it is present in both Ss and Sb while dislocations only occur in Sb, although it is likely that Ss91 contains a lower cordierite content (since XRD showed only small cordierite peaks) with the mullite being MgO-doped and the remaining MgO accommodated in triple junction glass (confirmed with EDS).[13] A further factor which may be significant here is the densification behaviour of these two composites. Sb91 reached high density (about 83% theoretical, Fig. 5) after 2 h at 1200°C so that little grain rearrangement was possible on further heating to 1400°C, leading to stress development. On the other hand, Ss91 reached only about 55% density (Fig. 5) after 2 h at 1200°C so that grain rearrangement but not growth can occur on further heating to 1400°C. The microstructure of a Ps91 composite (Fig. 8) after 2 h at 1450°C shows much larger mullite grains with the rod shape characteristic of mullite which has been liquid phase sintered as is the case at this temperature in this system.

In the *50% mullite* composites the very early stages of crystallisation were examined after 2 h at 1200°C. Typical glass ceramic microstructures were seen (Fig. 9) with mullite and cordierite crystals detected in a silica rich glass matrix in both Ss55 and Sb55 (compare Table 1) although the Ss composition appeared more crystalline. Lower maximum densities were achieved in Ss55 and Sb55 after 2 h at 1400°C than for either the 90% mullite or 90% cordierite composites (although they are still over 93% dense, Figs 3–5). While the reasons for this increased porosity are not obvious, three possibilities can be considered. First, vapour species evolved from the starting materials such as OH from the cordierite or SO_2 from the aluminium sulphate precursor. Water evolution from cordierite glass and crystals is known to lead to large (5 μm) pores and bloating on high temperature sintering.[4] This explains the observation of such pores in the cordierite matrix of many samples [e.g. see Fig. 13(b)] but does not seem to explain the behaviour of the Ss55 and Sb55 composites compared e.g. to those with higher cordierite contents. Second, the different thermal expansions of the

Fig. 8. SEM image of Ps91 after 2 h at 1450°C (thermally etched 30 min at 1300°C) showing the more characteristic rod-like structure of liquid phase sintered mullite.

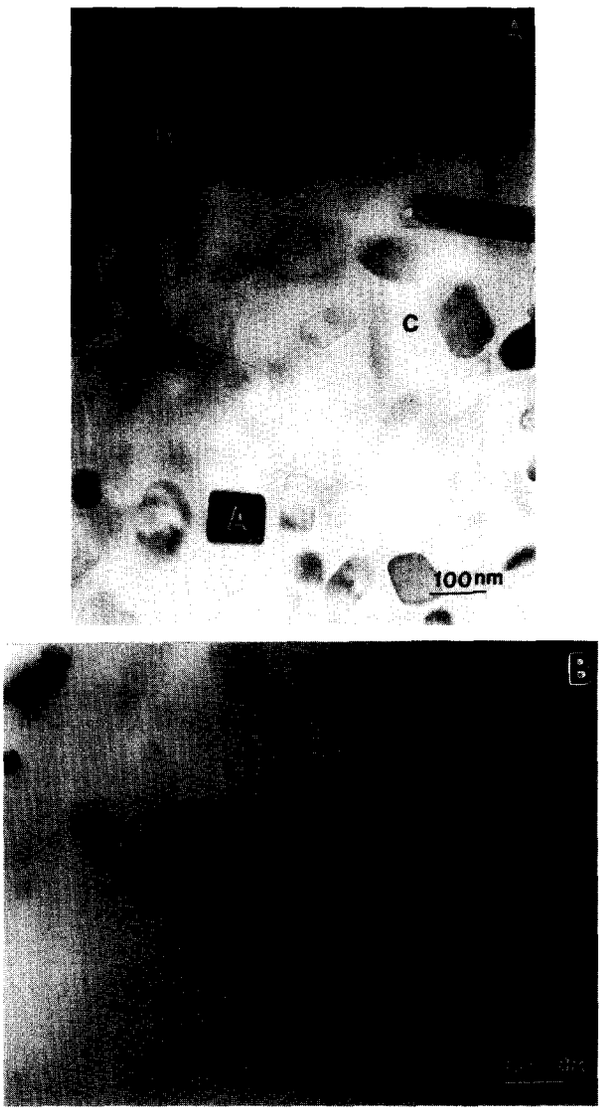

Fig. 9. BF-TEM images of early stages of crystallisation after 2 h at 1200°C (a) Ss55 and (b) Sb55. The more advanced state of crystallisation in Ss55 is clear supporting the XRD data in Table 1. The phases in Ss 55 identified by EDS are mullite (A), MgO-doped β-cordierite with its characteristic rounded, dendritic morphology (B), and silica rich glass (C).

Table 1. Results of XRD analysis

Composition	*1100°C*	*1200°C*	*1300°C*	*1400°C*	*1450°C*
Ss19	m′,c′,s,γ	m,c′,cr,γ	m,c	m,c	m,c
Ss55	m′,c′,s,γ	m,c′,cr,γ	m,c	m,c	m,c
Ss91	m′,c′,γ	m,c′,γ	m,c	m,c	m
Sb19	γ	m,c′,s,cr,γ	m,c	m,c	m,c
Sb55	s,γ	m,c′,s,cr,γ	m,c	m,c	m,c
Sb91	γ	m,c′,cr,γ	m,c	m,c	m
Ps19	—	—	m,c	m,c	m,c
Ps55	—	—	m,c	m,c	m,c
Ps91	—	—	m,c	m,c	m

m : orthorhombic mullite, m′ : tetragonal mullite, c : α-cordierite, c′ : β-cordierite, cr : cristobalite, s : (Mg-Al) spinel, γ : γ-alumina.

mullite and cordierite grains. A third possibility is that in the precursor-derived systems (Sb55 and Ss55) the scale of mixing (nm for Ss, μm for Sb) and the need to form equal amounts of two phases means that in the competition for mass transport densification misses out. Figure 10 shows the dense microstructure of Ps55 composite sintered 2 h at 1450°C. This sample has been severely etched in order to separate the fine cordierite matrix from the coarser mullite. This type of microstructure with mullite particle–particle contacts forming agglomerates was suggested by Hodge[2] to form by solid state sintering of mullite at these temperatures. TEM (Fig. 11) reveals the large ($\approx$1–3 μm) mullite grains surrounded by the fine ($\approx$0·4 μm) cordierite grains with their characteristic mottled contrast. In the powder route composites (Ps) the density obtained after the cordierite melts at 1450°C (2·75 g cm^{-3}) is comparable with the density obtained from composites derived from the precursor route (Sb and Ss) after 2 h at 1400°C (2·71 g cm^{-3}). However, the density at 1400°C (2·21 g cm^{-3}) before liquid formation in the Ps composites is comparable to the precursor route composite densities after 2 h at 1100–1200°C (1·9–2·3 g cm^{-3}). This illustrates the importance of liquid formation on densification in these systems.

The *10% mullite* composites after 2 h at 1400°C had the expected microstructure of fine (0·5μm) mottled cordierite grains and occasional angular mullite (illustrated for Sb19 in Fig. 12).

TEM revealed glass at triple junctions in all samples but not penetrating along grain boundaries. EDS showed the glass to be silica rich with both Mg and Al present.[13] Additionally, in Ss compositions Ca, K and S peaks were detected arising from impurities in the starting materials. These contaminants effect the wetting behaviour of the liquid during densification and will be discussed in detail in a forthcoming publication.[19]

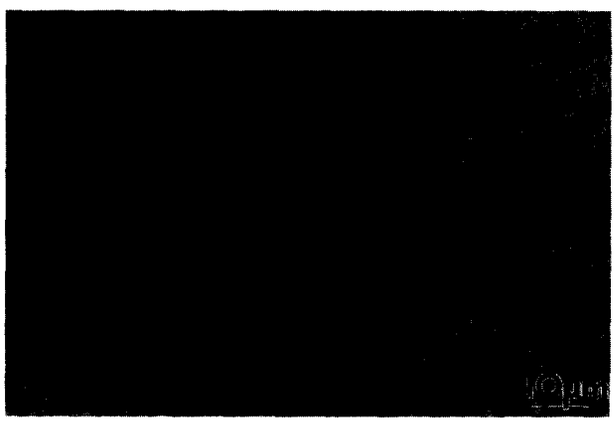

Fig. 10. SEM image of Ps55 composite at 1450°C for 2 h chemically etched with HF 5% for 58s.

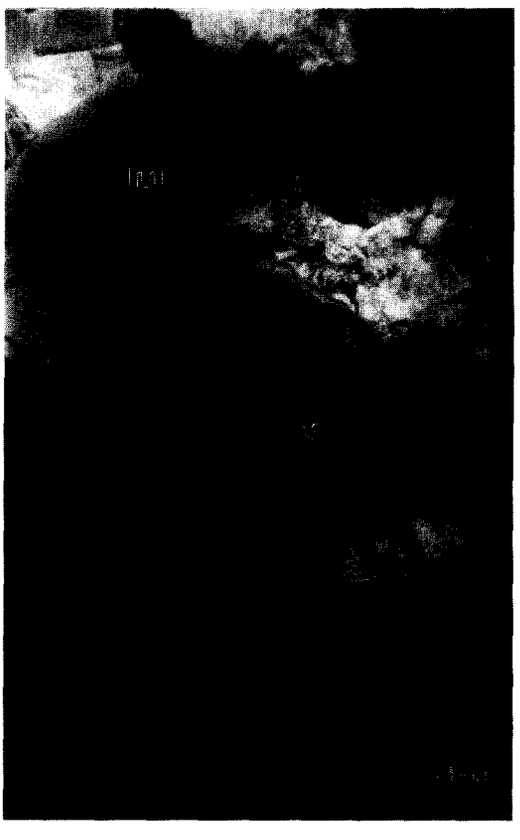

Fig. 11. BF-TEM image of Ps55 composite, sintered 2 h at 1450°C, c: cordierite and m: mullite.

Fig. 12. BF-TEM image of Sb19 sintered 2 h at 1400°C c: cordierite and m: mullite.

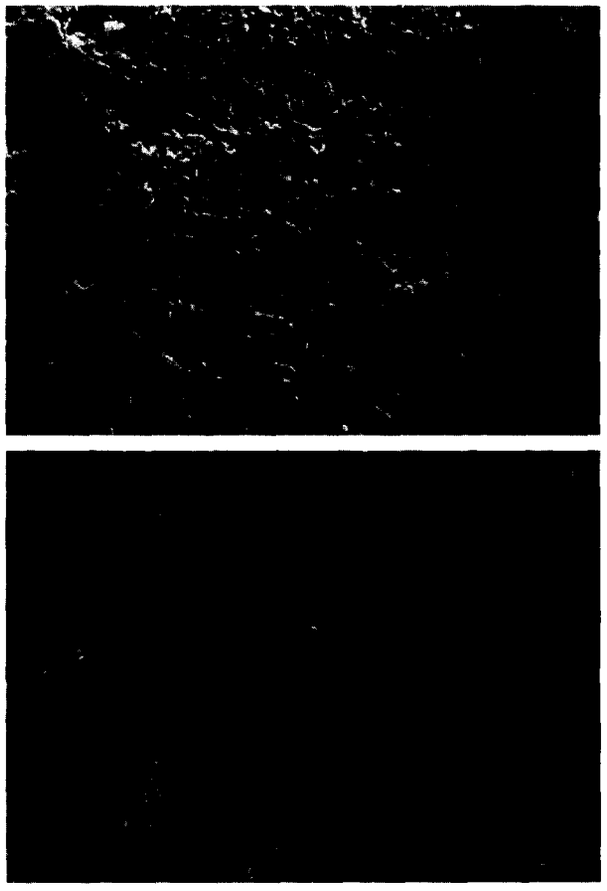

Fig. 13. Bend test fracture surfaces of (a) Sb91 and (b) Sb55, sintered 2 h at 1400°C. Note the pores in Sb55.

3.4 Mechanical properties

3.4.1 Bend strength

The bend strengths of pure, polycrystalline and dense mullite and cordierite are in the range 280–405MPa[20] and 98–138MPa,[21] respectively, dependent predominantly on grain size and porosity levels. Results of room-temperature 4-point-bend testing of Sb and Ps composite bars sintered at 1400° and 1450°C are shown in Table 2. Strengths are not high, ranging from 109–150MPa and do not follow the expected increase with mullite content due to the influence of porosity. Only for composites with 90wt% mullite is there a significant strength difference between the Sb and Ps samples, which can be attributed to the much greater level of porosity in the latter. The effect of grain size on the strength is not significant since measured grain sizes were similar. Figure 13(a) shows a typical fracture surface of Sb91 after 2 h at 1400°C revealing high density consistent with Fig. 5 and freedom from bulk defects related to compaction behaviour or preferential densification of agglomerates. With increased cordierite content (from 10 to 50wt %) but the same heat treatment $\approx 1{\cdot}5\mu$m pores develop in the microstructure [Fig. 13(b)] consistent with the density data (Fig. 4) and porosity increases from 3·3% (Sb91) to 8·2% (Sb55). These pores in Sb55 will act as fracture origins since many of them are more than twice the average grain size of $\approx 0{\cdot}6\,\mu$m (Table 2). Examination of the pressed surfaces of green bars of Sb and Ps composites (Fig. 14) showed that in Sb nearly all agglomerates had been crushed giving a smooth topography, while Ps contains large agglomerates (≈ 1–$5\,\mu$m) and a rough topography. Formation of crushable, soft agglomerates in Sb composites can be attributed to the low calcination temperature (600°C) and the presence of weak glassy phase while in Ps composites hard agglomerates are formed due to the high calcination temperatures and resulting fully crystallised powders (1700° and 1300°C for mullite and cordierite powders, respectively).

Similar low strength values were obtained by Anderson *et al.*[1] for mullite/cordierite composites made from mixed powders ranging from 162MPa for 10% mullite to 170MPa for 75% mullite although Ismail *et al.*[6] obtained strengths ranging from 250–322MPa in ceramics derived from Sb type powders. The porosity values in the ceramics of the latter group were, however, much lower than those of this and Anderson *et al.*'s study.[1]

3.4.2 Hardness and toughness

Pure, fully dense, polycrystalline mullite has a low toughness (2–3MPam$^{1/2}$) and a hardness of about 11GPa [22] whereas polycrystalline cordierite has similar toughness and about 8GPa hardness.[21] Toughness and hardness data for Sb and Ps composites are shown in Table 3. The toughness values are fairly consistent (if low) at about 2MPam$^{1/2}$ and the hardnesses in general show the expected increase with mullite content except for Ps91 which has a high porosity value (11·8%). The lower

Table 2. Flexural strength, porosity and grain size of composites sintered 2 h at 1400/1450°C and derived from precursor (Sb) and powder (Ps)

Property	*Composite type*	*Mullite content (wt%)*		
		10	*50*	*90*
Porosity (%)	Sb	7·4 ± 0·4	8·2 ± 0·2	3·3 ± 0·1
	Ps	4·6 ± 0·3	10·7 ± 1·2	19·1 ± 1·7
Average grain size (μm)	Sb	0·5 ± 0·1	0·6 ± 0·15	1·2 ± 0·21
	Ps	0·8 ± 0·12	1·5 ± 0·1	1·6 ± 0·25
Flexural strength (MPa)	Sb	119 ± 45	113 ± 42	150 ± 50
	Ps	131 ± 32	110 ± 40	109 ± 35

Table 3. Fracture toughness, hardness, porosity and grain size of composites sintered 2 h at 1400/1450°C and derived from precursor (Sb) and powder (Ps) routes

Property	*Composite type*	*Mullite content (wt%)*		
		10	*50*	*90*
Porosity (%)	Sb	6·1[a]	5·7	2·5
	Ps	3·05	3·24	11·8
Average grain size (μm)	Sb	0·5 ± 0·1	0·6 ± 0·15	1·2 ± 0·21
	Ps	0·8 ± 0·12	1·5 ± 0·1	1·6 ± 0·25
Toughness (MPa $m^{1/2}$)	Sb	1·5 ± 0·3	1·6 ± 0·5	2·2 ± 0·3
	Ps	2·0 ± 0·2	2·1 ± 0·3	1·4 ± 0·3
Hardness (GPa)	Sb	7·0 ± 0·8	7·6 ± 1·4	10·8 ± 0·9
	Ps	8·7 ± 1·0	9·3 ± 0·5	7·5 ± 1·0

[a]Only one sample was measured so ranges not applicable.

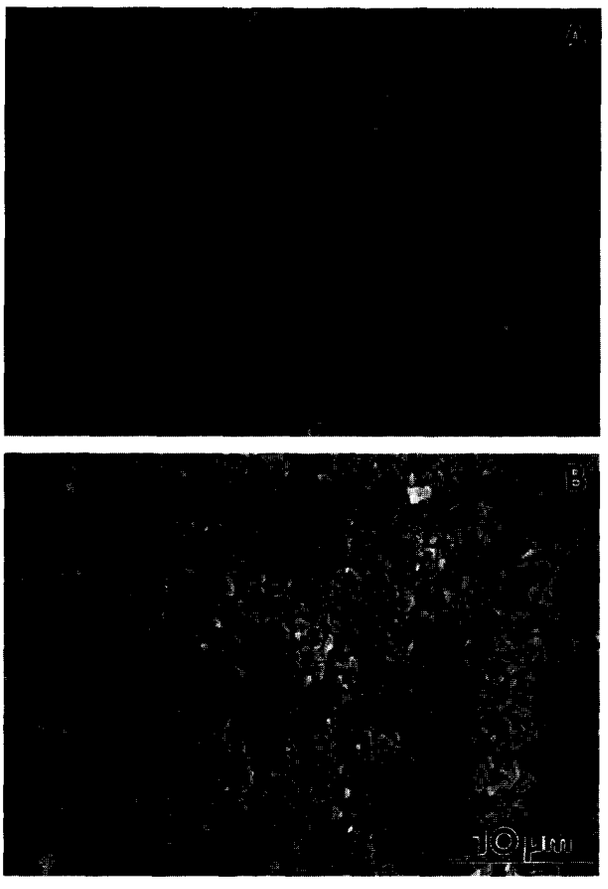

Fig. 14. SEM images of green pellet surfaces of (a) Sb91 and (b) Ps91 composites, uniaxially pressed at 250MPa. Note the presence of hard agglomerates in Ps91.

hardness and toughness of Sb composites compared to Ps is due to the higher porosity and glass content. Sb19 and Sb55 composites contain higher porosities (6·1 and 5·7%, respectively) than Ps19 and Ps55 (3·05 and 3·24%, respectively). Similar values and trends have been obtained for toughness in mullite/cordierite composites by others[1,4] although few hardness values have been presented. The dependence of toughness (and strength) on porosity in ceramics has been discussed by Lee and Rainforth.[15] One method of increasing toughness in high mullite composites would be to coarsen the microstructure allowing the characteristic elongated grain structure of mullite to develop. Examination of cracks traversing microstructures reveals both inter- and trans-granular failure of mullite and cordierite grains. Fig. 15 reveals the relatively straight crack path from an indent through the fine cordierite matrix in Ps19 sintered 2 h at 1450°C. However, a large ($\approx 4\ \mu$m) mullite grain does block crack propagation so that some toughening mechanisms are operative.

3.5 Dielectric properties

The dielectric constants of pure mullite and cordierite derived from boehmite, colloidal silica and magnesium nitrate were measured as 7·21 and 5·02, respectively. These values are in close agreement with other published values.[23,24] Since the presence of air (dielectric constant = 1) in pores will lower

Fig. 15. Vickers indentation crack path in Ps19 sintered 2 h at 1450°C and chemically etched with 5% HF for 58 s. Note the blunting effect of the large mullite particle.

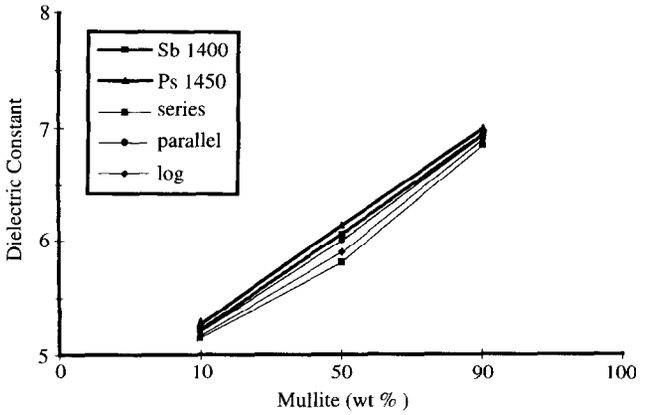

Fig. 17. Room temperature dielectric constant of mullite–cordierite composites at 1 MHz after correction for porosity.

the dielectric constant of mixed mullite–cordierite composites it is important to correlate dielectric data and pore levels. In Sb composites by increasing the mullite content from 10 to 90 wt%, the dielectric constant increases at a constant rate (Fig. 16) attributable to the decreased porosity (from 5·8 to 2·3%, Table 4) and increased mullite content. In Ps composites a similar rate of increase occurs from 10–50% mullite but it then levels off on going to 90% mullite due to the increased porosity (3·3 to 11·2%, Table 4). The lower dielectric constant of Sb composites (10 and 50 wt% mullite) and greater deviation from the mixing rule predictions are due to the presence of porosity. By normalising the dielectric constants for the composites to zero porosity (Fig. 17) a close correlation to the

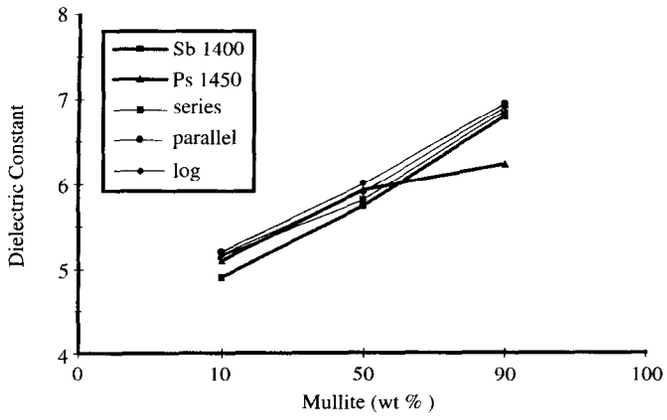

Fig. 16. Room temperature dielectric constant of mullite–cordierite composites measured at 1 MHz.

Table 4. Porosity (%) of the Sb and Ps composites used for dielectric constant measurements

Mullite content (wt %)	*Sb*	*Ps*
10	5·8[a]	3·1
50	5·2	3·3
90	2·3	11·2

[a]Only one sample was measured so ranges not applicable.

mixing rules[1] is seen and to the data obtained for mullite/cordierite composites by others.[1,4,6] The dielectric constants of Ps composites are higher than the values calculated from the mixing rules believed due to the incongruent melting of cordierite at 1450°C which converts to mullite and liquid so that the content of mullite in Ps composites is higher than expected. The presence of the glass detected at triple junctions in all samples by TEM does not have a critical effect on the dielectric constant of Sb composites, for two reasons. First, the amount of glass is low, only occurring isolated at triple junctions and not being connected throughout the microstructure. Second, the dielectric constant of the glass is likely to be relatively high due to the presence of Mg and Al in it detected by EDS. For most glasses, the dielectric constant at room temperature is linearly related to the density, which in turn can be related to composition.[25,26] Thus, the presence of Mg and Al ions causes increased glass density, due to the higher density of MgO and Al_2O_3 oxides than SiO_2, and correspondingly increased dielectric constant.

4 Conclusions

Crystallisation occurs more readily in mullite–cordierite composites made from powders derived from aluminium sulphate precursors due to the finer scale of mixing of the starting materials. The earlier crystallisation then leads to lower densities since densification via viscous flow is more limited. Various phases (e.g. spinel, γ-alumina, cristobalite) crystallise in the sol–gel precursor powders but after 2 h at 1400°C all are mullite and cordierite. XRD of those composites initially containing 10% cordierite after 2 h at 1450°C reveals only mullite although EDS showed the presence of MgO in solid solution with the mullite.

Composites made from precursor derived composites achieve higher density at lower temperatures than those made from mixed mullite and cordierite powders due to the higher reactivity of the powders and viscous flow of the glass present in them.

90% mullite composites derived from boehmite as the alumina source have larger grain sizes than when aluminium sulphate is used (over 1 μm compared to 0·5 μm). Mullite grains in boehmite-derived composites contain mullite cores which lead to a highly stressed microstructure containing many dislocations whereas sulphate-derived composites are stress free and the mullite grains contain MgO in solid solution. Higher levels of impurities (in particular S) were detected in sulphate-derived composites.

Mechanical properties could be related to the microstructures and their development through processing. Strength and hardness data could only be sensibly understood by correlating to composition, grain size *and* porosity measurements. Toughness values were all about 1·5–2MPam$^{1/2}$.

Dielectric data scaled well with the mixing rules for composites if normalised for porosity content.

References

1. Anderson, R. M., Gerhardt, R., Wachtman, J. B., Onn, D. and Beecher, S., Thermal, mechanical, and dielectric properties of mullite–cordierite composites. *Advances in Ceramics*, 1989, **26**, 265–277.
2. Hodge, J. D., Densification and microstructural aspects of mullite–cordierite ceramics. *Advances in Ceramics*, 1986, **19**, 117–129.
3. Hodge, J. D., Microstructure development in mullite–cordierite ceramics. *J. Am. Ceram. Soc*, 1989, **72**(7), 1295–1298.
4. Mussler, B. H. and Shafer, M. W., Preparation and properties of mullite–cordierite composites. *Bull. Am. Ceram. Soc*, 1984, **63**(5), 705–710.
5. Chandran, R. G., Patil, K. C. and Chandrappa, G. T., Combustion synthesis, characterization, sintering and microstructure of mullite–cordierite composites. *J. Mater. Sci. Letters*, 1995, **14**, 548–551.
6. Ismail, M. G. M. U., Tsunatori, H. and Nakai, Z., Preparation of mullite–cordierite composite powders by the sol–gel method: its characteristics and sintering. *J. Am. Ceram. Soc*, 1990, **73**(3), 537–543.
7. Schneider, H. and Rymon-Lipinski, T., Occurrence of pseudotetragonal mullite. *J. Am. Ceram. Soc*, 1988, **71**(3), C162–C164.
8. Ismail, M. G. M. U., Tsunatori, H. and Nakai, Z., Preparation of MgO-doped mullite by sol–gel method, powder characteristics and sintering. *J. Mater. Sci*, 1990, **25**, 2619–2625.
9. Glendenning, M. D. and Lee, W. E., Microstructural development on crystallising hot-pressed pellets of cordierite melt-derived glass containing B_2O_3 and P_2O_5,. *J. Am. Ceram. Soc.*, 1996, **79**(3), 705–713.
10. Schreyer, W. and Schairer, J. F., Compositions and structural states of anhydrous Mg-cordierites: a reinvestigation of the central part of the system MgO-Al_2O_3-SiO_2. *J. Petrol*, 1961, **2**(3), 324–406.
11. Smart, R. M. and Glasser, F. P., Stable cordierite solid solutions in the system: composition, polymorphism and thermal expansion. *Science of Ceramics*, 1977, **1**, 256–263.
12. Schreyer, W. and Schairer, J. F., Metastable solid solutions with quartz-type structures on the join SiO_2–$MgAl_2O_4$. *Zeitsch. Kristall*, 1961, **116**, 60–82.
13. Ebadzadeh, T., Processing, microstructure and properties of mullite–cordierite composites, Ph. D. Thesis, University of Sheffield, 1996.
14. Brindley, G. W. and Nakahira, M., The kaolinite reaction series: I. a survey of outstanding problems. *J. Am. Ceram. Soc*, 1959, **42**(7), 311–314.
15. Lee, W. E. and Rainforth, W. M., *Ceramic Microstructures: Property Control by Processing*. Chapman & Hall, London, 1994.
16. Evans, A. G. and Charles, E. A., Fracture toughness determination by indentation. *J. Am. Ceram. Soc*, 1976, **59**(7-8), 371–372.
17. Kazakos-Kijowski, A., Komarneni, S. and Roy, R., Multi-phasic nano-composite sol–gel processing of cordierite. *Mater. Res. Soc. Symp. Proc*, 1988, **121**, 245–250.
18. Wei, W.-C. and Halloran, J. W., Phase transformation of diphasic aluminosilicate gels. *J. Am Ceram. Soc*, 1988, **71**(3), 166–172.
19. Ebadzadeh, T. and Lee, W. E., Influence of impurities on wetting of mullite by cordierite liquid. *J. Mater. Sci. Lett.*, 1998, to be published.
20. Ismail, M. G. M. U., Nakai, Z. and Somiya, S., Microstructure and mechanical properties of mullite prepared by the sol–gel method. *J. Am. Ceram. Soc*, 1987, **70**(1), C7–C8.
21. Suzuki, H., Ota, K. and Saito, H., Mechanical properties of alkoxy-derived cordierite ceramics. *J. Mater. Sci*, 1988, **23**, 1534–1538.
22. Schneider, H., Okada, K. and Pask, J. A., *Mullite and Mullite Ceramics*. J. Wiley, New York, NY, 1994.
23. Suzuki, H., Saito, H. and Hayashi, T., Thermal and electrical properties of alkoxy-derived cordierite ceramics. *J. Euro. Ceram. Soc*, 1992, **9**, 365–371.
24. Ismail, M. G. M. U., Nakai, Z., Ohira, H. and Somiya, S., Preparation and characterisation of mullite containing materials. In *Ceramic Powder Science*, Vol. 1. ACerS, OH, 1988, pp. 1108–1114.
25. Stevels, J. M., *Progress in the Theory of the Physical Properties of Glass*. Elsevier, London, 1948.
26. Espe, W., *Materials of High Vacuum Technology, Vol. 2: Silicates*, Chs 10–12. Pergamon Press, Oxford, 1968.